Title
Multimodality endoscopic optical coherence tomography and fluorescence imaging technology for visualization of layered architecture and subsurface microvasculature.

Journal
Optics Letters, 43(9)

ISSN
0146-9592

Authors
Li, Yan
Jing, Joseph
Yu, Junxiao
et al.

Publication Date
2018-05-01

DOI
10.1364/ol.43.002074

Peer reviewed

HHS Public Access

Author manuscript

Opt Lett. Author manuscript; available in PMC 2019 May 01.

Published in final edited form as:

Opt Lett. 2018 May 01; 43(9): 2074–2077. doi:10.1364/OL.43.002074.

Multimodality Endoscopic Optical Coherence Tomography and Fluorescence Imaging Technology for Visualization of Layered Architecture and Subsurface Microvasculature

YAN LI[1,2], **JOSEPH JING**[1,2], **JUNXIAO YU**[1,2], **BUYUN ZHANG**[1], **TIANCHENG HUO**[1], **QIANG YANG**[1], and **ZHONGPING CHEN**[1,2,*]

[1]Department of Biomedical Engineering and Beckman laser institute, University of California, Irvine, Irvine, California 92617, USA

[2]Department of Biomedical Engineering, University of California, 5200 Engineering Hall, Irvine, California 92697, USA

Abstract

Endoscopic imaging technologies, such as endoscopic optical coherence tomography (OCT) and near infrared (NIR) fluorescence have been used to investigate vascular and morphological changes as hallmarks of early cancer in the gastrointestinal (GI) tract. Here, we developed a high speed multimodality endoscopic OCT and fluorescence imaging system. Using this system, the architectural morphology and vasculature of the rectum wall were obtained simultaneously from a Sprague Dawley (SD) rat *in vivo*. This multimodality imaging strategy in a single imaging system permits the use of a single imaging probe, thereby improving prognosis by early detection and reducing costs.

Keywords

(110.4500) Optical coherence tomography; (260.2510) Fluorescence; (110.4190) Multiple imaging; (170.2150) Endoscopic imaging; (170.2680) Gastrointestinal

Globally, there are ~1.4 million new cases and 694,000 deaths from colorectal cancer annually, which is the third most common type of cancer consisting of 10% of all cancer cases [1]. Currently, a clinician routinely applies endoscopy to visualize the rectum wall for diagnosis of the GI disease [2]. Due to the lack of depth information and limited sensitivity for the vascular lesion, the disorders in which early epithelial dysplastic changes are usually not clearly visible at endoscopy. In recent decades, more and more novel endoscopic imaging technologies [3–10] have been developed to visualize the sub-layered morphology and subsurface vascular network for providing necessary information in order to assess disease stage or progress and plan treatment therapies. For example, endoscopic ultrasound (EUS) [4, 11] imaging allows a clinician to obtain images of the GI tract and the surrounding tissue and organs with an imaging depth of ~7 mm and a resolution of ~150 μm. However, many disorders of the GI tract, cancer in particular, arise within the mucosa.

*Corresponding author: z2chen@uci.edu.

Therefore, limited by the resolution of the EUS, it is difficult to detect changes in the early stage of GI disease. Recently, endoscopic OCT [12–16] which is capable of providing high-resolution cross-sectional images architectural- and cellular-tissue microstructure has been widely applied to image of the esophagus, stomach, small and large intestine, and biliary and pancreatic ducts. In addition, endoscopic Doppler OCT technology [15, 17, 18] has been applied in endoscopic imaging to visualize vascular networks without any exogenous fluorescent agent. However, limited by the phase stability of the system and movement from the imaging probe, the reconstructed Doppler OCT images often contain motion artifacts and have relatively low sensitivity for microvasculature due to random and slow flow speed of capillary. Another endoscopic angiography technology is NIR fluorescence imaging [3, 5, 19–21] with indocyanine green (ICG), which provides high resolution microvasculature imaging and has been used clinically to observe a variety of vascular lesions, such as detecting abnormal submucosal vascularization in tumor lesions. By using different kinds of endoscopic imaging technology, the clinician is able to obtain various features of the biological tissue [6]. Therefore, in the clinic, several endoscopic imaging technologies are often needed to obtain enough features of the biological tissue for accurate diagnosis. The usage of different technologies increases the cost and time of imaging for hospitals and patients. Recently, several groups already reported integrated OCT and fluorescence imaging system [6, 22–27], and these works represent a significant step forward for the characterization of GI disease. However, *in vivo* mapping of microvascular network and characterization of tumor angiogenesis in GI remains a challenge. The multimodality endoscopic OCT and fluorescence imaging system for mapping microvascular network requires a combination of high speed, high spatial resolution, uniform scanning system, and FDA approved contrast agent. Although current reported imaging system can achieve some of the above attribute, none of the reported system has the combined attributes to be effective for high speed *in vivo* mapping of microvascular network.

Here, we report a high-speed multimodality endoscopic OCT and fluorescence imaging system that overcome current system limitations. Our endoscopic OCT and fluorescent system is based on a distal scanning method. A micro motor was used to drive the mirror with high speed to provide uniform rotation for resolving the microvasculature with high spatial resolution. In addition, we used an FDA approved contrast agent to visualized microvascular network with high sensitivity. A B-scan rate up to 100Hz (1000 A-lines/B-scan) was achieved. Three-dimensional (3D) OCT and fluorescence images of rectum from a rat were demonstrated. For OCT images, the well-defined layered architecture can be identified clearly. For fluorescence images, we used the FDA-approved ICG which is excited by rays at a wavelength of 785 nm to emit fluorescence at a wavelength of 815 nm in the infrared (IR) range as a fluorescent marker to target vasculature. Our results indicate that the multimodality imaging system allows for better identification of the layered morphology and vascular network of the GI tract, which may provide new opportunities for detecting and monitoring GI diseases.

Figure 1 illustrates the overall setup of the multimodality imaging system. A wavelength division multiplexer is utilized to combine the OCT and fluorescence laser beams together. For OCT, a 1310 nm Micro-Electro-Mechanical (MEMS)-tunable Vertical Cavity Surface Emitting Laser (VCSEL) swept source laser with a sweeping rate of 100 kHz is used. For

fluorescence imaging, a 785-nm semi-conductive CW laser (IS785–50 IR, Meshtel) is used as the excitation source, which corresponds to the excitation peak of the ICG. A double clad fiber (DCF) coupler that combines a double-clad fiber (single mode core Ø 9 μm with 0.12 NA, surrounded by a multimode inner cladding Ø 105 μm with 0.2 NA) with a standard step-index multimode fiber, is incorporated to transmit excitation light and collect emission light. For transmission, the combined beams go through the core of the DCF from port A to port S, and the small diameter of the single mode core contributes to high fluence on surface tissue, which enables a high efficiency excitation. The emission light will come back from the first clad of the DCF and core (port S) to a multimode fiber (port B) whose larger diameter and higher numerical aperture (NA) enhance the capability of collecting emission light, which is then detected by a photomultiplier tube (PMT, Hamamatsu, Photosensor module: H10722–20).

A multimodality OCT and fluorescence imaging probe based on a micro motor was designed and implemented, as is shown in Figure 2 (a). The combined beams propagate through the single mode core of the DCF, focused by a 1 Grin-lens (Aviation Magneto Optical Sensor Corp.) and reflected by a rod mirror with a diameter of 1 mm at an angle of 45°, then to the tissue surface. In order to keep the optical beams accurately aligned with mirror that attached the shaft of micro motor, we glued a ferrule with the same outer diameter as the micro motor outside of the Grin-lens. A micro motor with a diameter of 2.4 mm was used to rotate the rod mirror at a frame rate of 100 images per second. By pulling back the imaging probe with a speed of 1 mm/s, a helical scan pattern was performed, and then the 3D OCT (axial resolution: 8.7 μm, lateral resolution: 30 μm) and fluorescence images (lateral resolution: 27 μm) were obtained.

We imaged the rectum of a SD rat. The rat was placed in a closed plexiglass chamber into which 5% isoflurane in oxygen was allowed to flow in order to induce general anesthesia for restraint during the procedure. Following the gas anesthetic induction, the rat was removed from the chamber and an IP injection of ketamine hydrochloride (87mg/kg) and xylazine (10mg/kg) was administered through a 27G needle. After the rat was anesthetized, we performed enemas to clean the rectum and then inserted a balloon to inflate the rectum wall. After that, ICG (1. 5mg/Kg) was injected via tail vein to target blood vessels of the rectum wall; then the *in vivo* experiment was performed. All methods were carried out in accordance with the University of California, Irvine (UCI) Institutional Review Board (IRB) and the Institutional Biosafety Committee (IBC). All experimental protocols were approved by the UCI IBC under protocol #2016–3198.

Figures 3 shows the representative combined OCT (inner) and fluorescence (outer) B-scan images of the rectum along pullback direction. We acquired ~ 2400 B-scan OCT and fluorescence images with a pullback speed of 1mm/s. From the inner images, the typical layered architecture can be identified, indicated by the white dashed box. In addition, several black holes were found, which corresponds to blood vessels. The black shadow at the 8 o'clock direction was caused by the lead of the micro-motor. The white and yellow arrows represent the OCT images of nylon tubing outside the micro-motor and balloon catheter, respectively. For fluorescence imaging, we injected ICG into the blood via the tail vein of

the rat. Therefore, all the blood vessels were targeted by ICG. That means the region which contains blood vessel will correspond to a high intensity in the fluorescence images.

Figures 4(b) and (c) show the reconstructed 2D OCT images along the pullback direction. Figure 4(d) shows the enlarged view of the dashed box in (b) in which the layered architecture can be visualized clearly (E, epithelium; tML, thin muscle layer; SM, submucosa; TML, thick muscle layer; S, serosa).

Figure 5 (a-f) shows representative 3D OCT, fluorescence and combined images. These results demonstrate that this multimodality endoscopic imaging system has the capability of visualizing the layered architecture and vasculature of the rectum wall simultaneously. Figure 5 (g) shows an unwrapped image from Figure 5 (e); the pattern of vasculature which is highly relevant to GI disease can be observed clearly. Figures 5 (h) and (i) are photos of the rat rectum. From Figure 5 (g), a big blood clot and three large vessel branches are clearly identified, which is consistent with the photos of the rectum indicated by green dashed box and arrows in Figure 5(h) and (i).

Endoscopic OCT and fluorescence imaging are non-invasive, non-ionizing imaging technology which are often used for the diagnosis and arrangement of GI disease. Here, we reported an endoscopic multimodality OCT and fluorescence imaging system which combines OCT and fluorescence imaging technology together to provide architectural morphology and molecular specifies of biological tissue simultaneously. The outer diameter of the imaging probe is around 3 mm, which is accessible through the accessory channel of the commercial endoscope. From the results obtained from an *in vivo* rat experiment, the typical layered architecture and microvasculature can be clearly identified. In the future, a diseased animal model will be studied for further verification of the performance of this multimodality endoscopic OCT and fluorescence.

In summary, this works presents *in vivo* multimodality endoscopic OCT and fluorescence imaging system. The images results demonstrate the ability for visualization of layered architecture and subsurface microvasculature, which has the potential to provide a new insight into the pathology of GI disease.

Acknowledgments.

Dr. Chen has a financial interest in OCT Medical Imaging, Inc., which, however, did not support this work.

Funding. National Institutes of Health (R01HL-125084, R01HL-127271, R01EY-026091, R01EY-021529, and P41EB-015890); Air Force Office of Scientific Research (FA9550–17-1–0193).

References

[1]. McGuire S World Cancer Report 2014. Geneva, Switzerland: World Health Organization, International Agency for Research on Cancer, WHO Press, 2015. Adv Nutr. 2016;7:418–9. [PubMed: 26980827]

[2]. Kronborg O, Fenger C, Olsen J, Jorgensen OD, Sondergaard O. Randomised study of screening for colorectal cancer with faecal-occult-blood test. Lancet. 1996;348:1467–71. [PubMed: 8942774]

[3]. Gostout CJ, Jacques SL. Infrared video imaging of subsurface vessels: a feasibility study for the endoscopic management of gastrointestinal bleeding. Gastrointest Endosc. 1995;41:218–24. [PubMed: 7789680]

[4]. Harewood GC. Assessment of clinical impact of endoscopic ultrasound on rectal cancer. Am J Gastroenterol. 2004;99:623–7. [PubMed: 15089892]

[5]. Iseki K, Tatsuta M, Iishi H, Sakai N, Yano H, Ishiguro S. Effectiveness of the near-infrared electronic endoscope for diagnosis of the depth of involvement of gastric cancers. Gastrointest Endosc. 2000;52:755–62. [PubMed: 11115912]

[6]. Yuan S, Roney CA, Wierwille J, Chen CW, Xu B, Griffiths G, et al. Co-registered optical coherence tomography and fluorescence molecular imaging for simultaneous morphological and molecular imaging. Phys Med Biol. 2010;55:191–206. [PubMed: 20009192]

[7]. Li Y, Gong XJ, Liu CB, Lin RQ, Hau W, Bai XS, et al. High-speed intravascular spectroscopic photoacoustic imaging at 1000 A-lines per second with a 0.9-mm diameter catheter. J Biomed Opt. 2015;20.

[8]. Li Y, Jing J, Qu YQ, Miao YS, Zhang BY, Ma T, et al. Fully integrated optical coherence tomography, ultrasound, and indocyanine green-based fluorescence tri-modality system for intravascular imaging. Biomedical optics express. 2017;8:1036–44. [PubMed: 28271001]

[9]. Qu YQ, Ma T, He YM, Yu MY, Zhu J, Miao YS, et al. Miniature probe for mapping mechanical properties of vascular lesions using acoustic radiation force optical coherence elastography. Scientific reports. 2017;7.

[10]. Li Y, Jing J, Heidari E, Zhu J, Qu Y, Chen Z. Intravascular Optical Coherence Tomography for Characterization of Atherosclerosis with a 1.7 Micron Swept-Source Laser. Sci Rep. 2017;7:14525. [PubMed: 29109462]

[11]. Mascagni D, Corbellini L, Urciuoli P, Di Matteo G. Endoluminal ultrasound for early detection of local recurrence of rectal cancer. Br J Surg. 1989;76:1176–80. [PubMed: 2688805]

[12]. Kirtane TS, Wagh MS. Endoscopic Optical Coherence Tomography (OCT): Advances in Gastrointestinal Imaging. Gastroenterology Research and Practice. 2014.

[13]. Kubo T, Akasaka T. Optical coherence tomography imaging: current status and future perspectives : Current and future developments in OCT. Cardiovasc Interv Ther. 2010;25:2–10. [PubMed: 24122426]

[14]. Standish BA, Lee KK, Mariampillai A, Munce NR, Leung MK, Yang VX, et al. In vivo endoscopic multi-beam optical coherence tomography. Phys Med Biol. 2010;55:615–22. [PubMed: 20071753]

[15]. Tsai TH, Ahsen OO, Lee HC, Liang K, Figueiredo M, Tao YK, et al. Endoscopic optical coherence angiography enables 3-dimensional visualization of subsurface microvasculature. Gastroenterology. 2014;147:1219–21. [PubMed: 25172015]

[16]. Yang VX, Tang SJ, Gordon ML, Qi B, Gardiner G, Cirocco M, et al. Endoscopic Doppler optical coherence tomography in the human GI tract: initial experience. Gastrointest Endosc. 2005;61:879–90. [PubMed: 15933695]

[17]. Chen Z, Milner TE, Dave D, Nelson JS. Optical Doppler tomographic imaging of fluid flow velocity in highly scattering media. Optics letters. 1997;22:64–6. [PubMed: 18183104]

[18]. Lee AMD, Ohtani K, MacAulay C, McWilliams A, Shaipanich T, Yang VXD, et al. In vivo lung microvasculature visualized in three dimensions using fiber-optic color Doppler optical coherence tomography. J Biomed Opt. 2013;18.

[19]. Alander JT, Kaartinen I, Laakso A, Patila T, Spillmann T, Tuchin VV, et al. A review of indocyanine green fluorescent imaging in surgery. Int J Biomed Imaging. 2012;2012:940585. [PubMed: 22577366]

[20]. Kim SY, Myung SJ. Optical molecular imaging for diagnosing intestinal diseases. Clin Endosc. 2013;46:620–6. [PubMed: 24340254]

[21]. Kimura T, Muguruma N, Ito S, Okamura S, Imoto Y, Miyamoto H, et al. Infrared fluorescence endoscopy for the diagnosis of superficial gastric tumors. Gastrointest Endosc. 2007;66:37–43. [PubMed: 17591472]

[22]. Ughi GJ, Wang H, Gerbaud E, Gardecki JA, Fard AM, Hamidi E, et al. Clinical Characterization of Coronary Atherosclerosis With Dual-Modality OCT and Near-Infrared Autofluorescence Imaging. JACC Cardiovascular imaging. 2016;9:1304–14. [PubMed: 26971006]

[23]. Mavadia J, Xi J, Chen Y, Li X. An all-fiber-optic endoscopy platform for simultaneous OCT and fluorescence imaging. Biomedical optics express. 2012;3:2851–9. [PubMed: 23162723]

[24]. Pahlevaninezhad H, Lee AM, Hohert G, Lam S, Shaipanich T, Beaudoin EL, et al. Endoscopic high-resolution autofluorescence imaging and OCT of pulmonary vascular networks. Optics letters. 2016;41:3209–12. [PubMed: 27420497]

[25]. Winkler AM, Rice PF, Weichsel J, Watson JM, Backer MV, Backer JM, et al. In vivo, dual-modality OCT/LIF imaging using a novel VEGF receptor-targeted NIR fluorescent probe in the AOM-treated mouse model. Molecular imaging and biology : MIB : the official publication of the Academy of Molecular Imaging. 2011;13:1173–82. [PubMed: 21042865]

[26]. Tumlinson AR, Hariri LP, Utzinger U, Barton JK. Miniature endoscope for simultaneous optical coherence tomography and laser-induced fluorescence measurement. Applied optics. 2004;43:113–21. [PubMed: 14714651]

[27]. Yoo H, Kim JW, Shishkov M, Namati E, Morse T, Shubochkin R, et al. Intra-arterial catheter for simultaneous microstructural and molecular imaging in vivo. Nat Med. 2011;17:1680–4. [PubMed: 22057345]

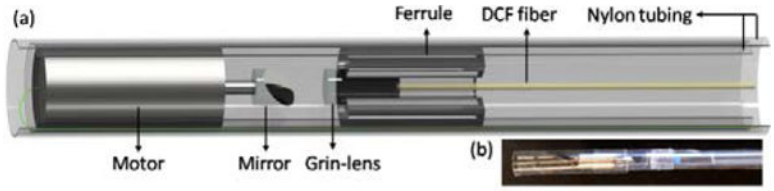

Fig 1.

Overall design of the multimodality system. WDM: wavelength division multiplexer. PMT: photomultiplier tube. DCF coupler: double clad fiber coupler.

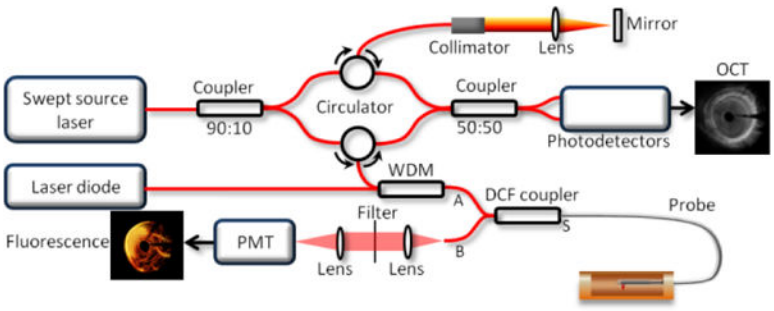

Fig 2.

Endoscopic multimodality OCT and fluorescence imaging probe. (a) Overall schematics. (b) Photo of the imaging probe.

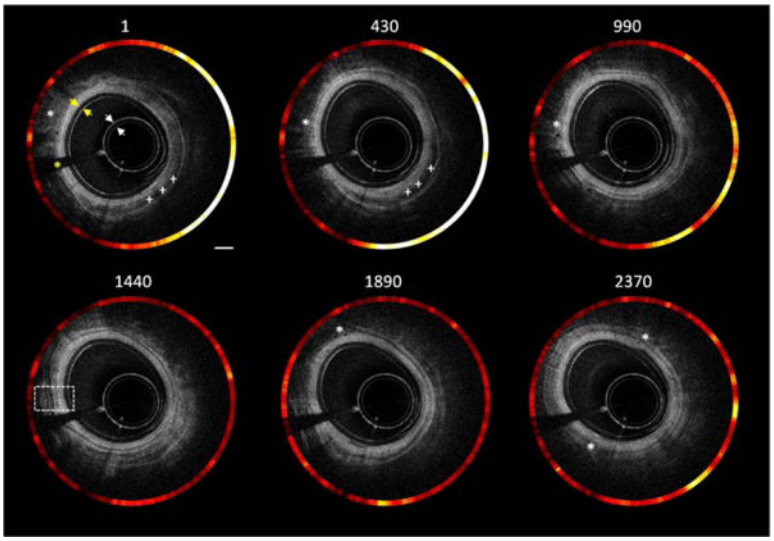

Fig 3.

Cross-sectional combined OCT and fluorescence images with different locations along pullback direction (see Visualization 1). White *: blood vessel; White +++: blood clot; Yellow *: black shadow which is caused by micro motor lead. White arrow: nylon tubing; yellow arrow: balloon catheter. Scale bar: 1 mm.

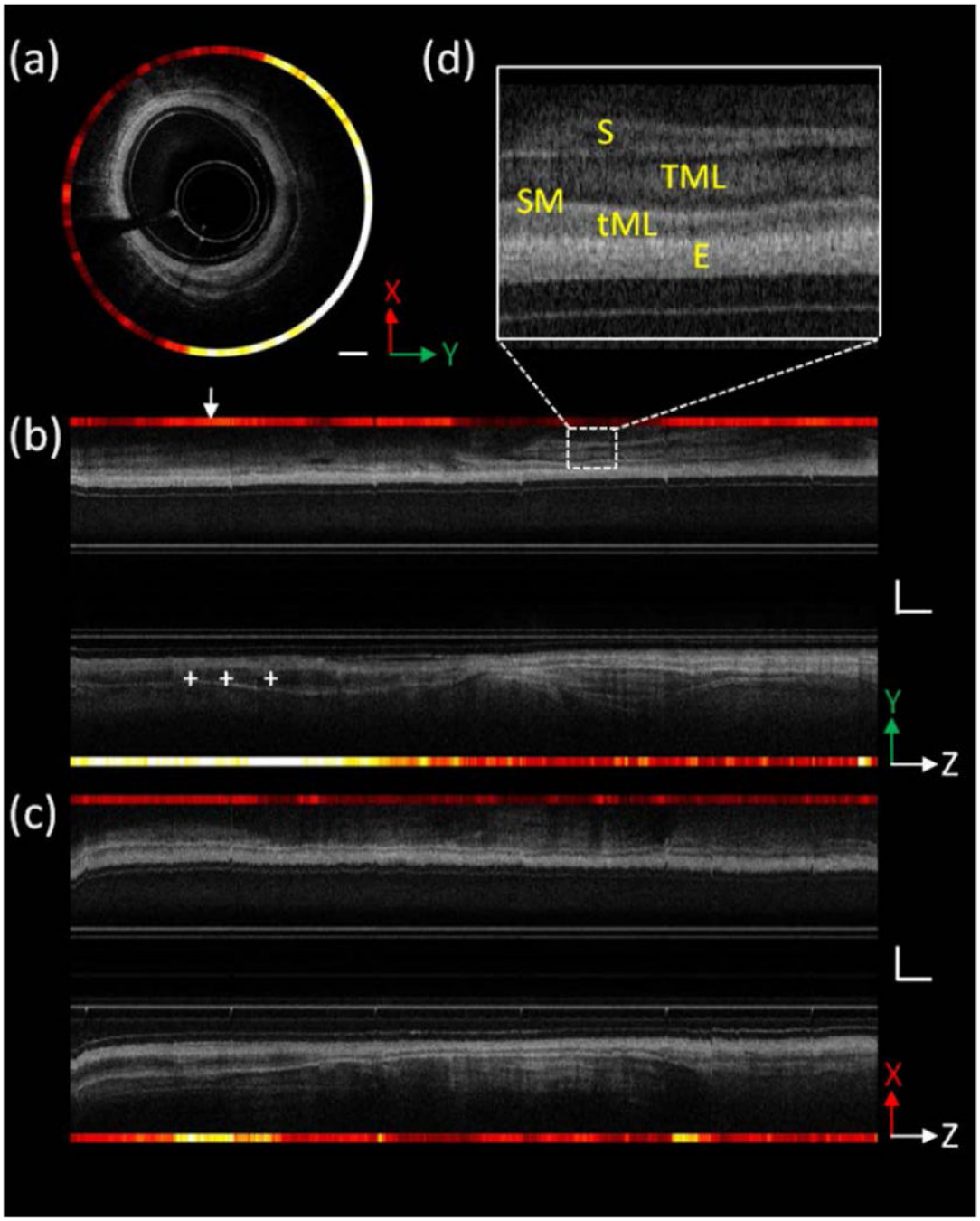

Figure 4.

Combined OCT and fluorescence images of the rat rectum. (a) Cross-sectional combined images of rectum, and the location is indicated by the white arrow in figure (b). (b) and (c) Cross-sectional combined images of rectum along pullback direction; section views are indicated by coordinates, respectively. (d) Enlarged view of the dashed box in (b) in which the different layered architecture of the rectum wall can be visualized clearly. E, epithelium; tML, thin muscle layer; SM, submucosa; TML, thick muscle layer; S, serosa. White Scale

bar: 1 mm. X and Y directions are perpendicular to each other, and both are in the vertical plane; Z: pullback direction.

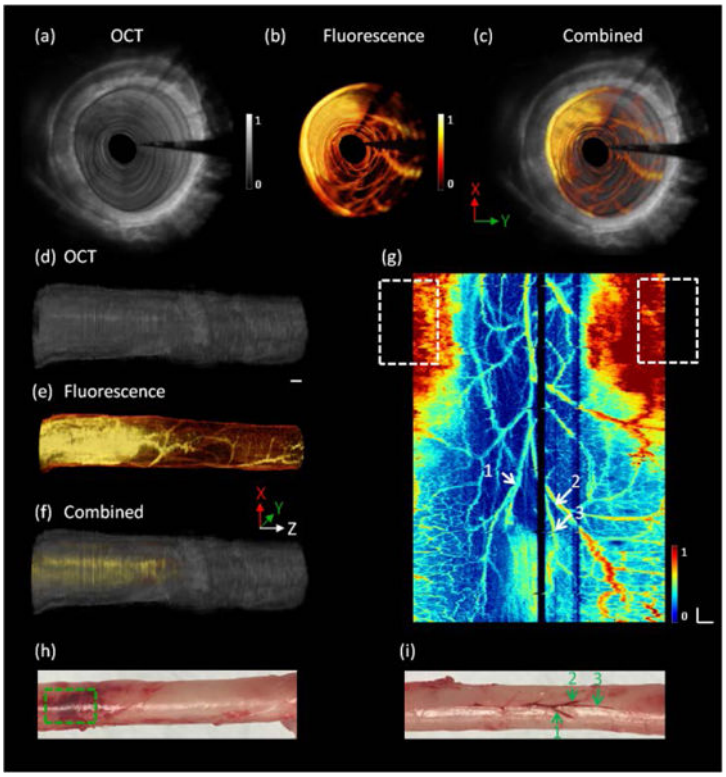

Figure 5.

3D endoscopic OCT and fluorescence images of the rat rectum. (a), (b) and (c) 3D fly-through OCT, fluorescence and combined images, respectively, inside the rectum wall (see Visualization 2). (d), (e) and (f) 3D OCT, fluorescence and combined images along the pullback direction. (g) En face unwrapped fluorescence image. (h) and (i) photos of the rat rectum. White and green arrows: major vessel branches. White and green dashed box: blood clot. X and Y directions are perpendicular to each other, and both are in the vertical plane; Z: pullback direction. White Scale bar: 1 mm.